Coupled Systems Mechanics, *Vol. 7, No. 3 (2018) 333-351*
DOI: https://doi.org/10.12989/csm.2018.7.3.333

Underwater explosion and its effects on nonlinear behavior of an arch dam

Melika Moradi, Seyyed Meisam Aghajanzadeh,
Hasan Mirzabozorg* and Mahsa Alimohammadi

Civil Engineering Department, KN Toosi University of Technology, Tehran, Iran

(Received November 18, 2017, Revised December 15, 2017, Accepted December 19, 2017)

Abstract. In the present paper, the behavior of the Karaj double curvature arch dam is studied focusing on the effects of structural nonlinearity on the responses of the dam body when an underwater explosion occurred in the reservoir medium. The explosive sources are located at different distances from the dam and the effects of the cavitation and the initial shock wave of the explosion are considered. Different amount of TNT are considered. Two different linear and nonlinear behavior are assumed in the analysis and the dam body is assumed with and without contraction joints. Radial, tangential and vertical displacements of the dam crest are obtained. Moreover, maximum and minimum principal stress distributions are plotted. Based on the results, the dam body responses are sensitive to the insertion of joints and constitutive model considered for the dam body.

Keywords: arch dam; underwater explosion; arch dam; damage plasticity; vertical joints

1. Introduction

Explosion is a chemical reaction, which converts the original material into the gas under very high temperature and pressure. The process occurs with extreme rapidity evolving a great deal of heat; and it is evident that these conditions will affect the surrounding medium. Explosion may happen underwater. Strategic value of the naval battles in the World War II was the main reason of underwater explosion researches and it has been the subject of many investigations since about 80 years ago.

Various theories of underwater explosions were collected by Cole (1948). He provided a simple and widespread formula for underwater explosion shock wave and its energy and impulse. In associated with modeling of this phenomenon, Kwon and Fox (1993) studied the nonlinear dynamic response of a cylinder subjected to side-on underwater explosion using both the experimental and numerical techniques. Sun and McCoy (1997) used the finite element package ABAQUS and a fluid-structure interaction code based on the DAA† to solve an UNDEX‡ analysis

*Corresponding author, Associate Professor, E-mail: Mirzabozorg@kntu.ac.ir
†Double Asymptotic Approximation
‡Under water Explosion

http://www.techno-press.org/?journal=csm&subpage=8 ISSN: 2234-2184 (Print), 2234-2192 (Online)

of a composite cylinder.

Qiankun and Ding (2011) investigated the dynamic responses of a ship section under non-contact underwater explosion load. They considered the incident shock wave, wave reflection by the free surface and seabed, bubble pulse, fluid-structure interaction and the bulk and local cavitation. Salajegheh *et al*. (2008) studied the hydrodynamic interaction of spar platforms with underwater explosion shock using a three-dimensional analysis of a spar finite element model coupled with a surrounding fluid subjected to a far-field underwater explosion causing the incident shock wave.

Modeling of underwater explosions and their effects on dams' responses has been considered by several researches in recent decades. Ghanaat *et al.* (2000) described the field measurements of the dam-water-foundation interaction phenomenon performed on the Longyangxia Dam. Furthermore, the dynamic response of concrete dams subjected to underwater contact explosion is studied by Yu (2009), who used the LS-DYNA software in his study. Xu and Liu (2008) studied the response of concrete gravity dams subjected to underwater explosions using the finite element model and; at last, a finite element modeling of arch dams subjected to underwater explosions was reported in recent years by Zhu and Feng (2012).

Although a more optimized form of concrete arch dams endures water pressure, and a larger stiffness resists the radial deformation, these advantages cause the weakness of impact resistance leading to disaster on the downstream area if the structure is wrecked (Feng *et al.* 2012). It seems that studying on this critical subject can be valuable.

In this paper, the finite element modeling of underwater explosion is considered and its effect on the Karaj Dam, a double curvature arch dam, is investigated. Various assumptions considering the dam body behavior, the location and the weight of the explosive material are studied and the results are compared.

2. Underwater explosion

When an underwater explosion occurs, a great amount of gas and energy is produced while as a result, a shock wave is generated. The produced compressive shock wave travels radially away from the explosion and the velocity of traveled shock wave is approximately equal to the velocity of sound in water. On the other hand, the bubbles form the explosive gases expand until the gas pressure reduces to zero. Subsequently, the fully expanded bubbles begin to collapse because of the hydrostatic pressure. A second shock wave is produced due to the high pressure while the bubbles are compressed. The fluid model should simulate the three phenomena occurred due to underwater explosion; the incident shock wave, the cavitation and the fluid-structure interaction. In numerical modeling, the shock wave within the fluid domain starts using initial conditions and cavitation occurs when the pressure in the surrounding water drops below the vapor pressure. As a result, the cavitation zone may cause reloading the structure, which may result in higher damage than the original pressure pulse caused by detonation of the charge (Qiankun and Gangyi 2011). In the current investigation, the effect of bubble formation is ignored and the initial shock wave of the explosion and the cavitation are considered.

2.1 Incident shock wave

The pressure load acting on the structure is a function of time and space. The incident shock

wave pressure can be approximated as an exponential function. This approximation is valid for spherical explosives of pressures greater than about one-third of the peak value. However, at later time the two deviations are observed; the first is an irregularity in the size and shape depending on the shape of the explosive; and the second one is more gradual decline in pressure than initial exponential decrease (Shah-Mohammadi and Mohammadi 2010). In this study, the pressure as a function of time after the arrival of the wave front for TNT is expressed as (Rajendran and Narasimhan 2006)

$$P(t) = P_{max} e^{-\frac{t-t_1}{\theta}} \tag{1}$$

$$P_{max} = 52.16 \left(\frac{W^{\frac{1}{3}}}{R} \right)^{1.13} \tag{2}$$

$$\theta = 96.5 W^{\frac{1}{3}} \left(\frac{W^{\frac{1}{3}}}{R} \right)^{-0.22} \tag{3}$$

where, P_{max} is the peak pressure of the shock wave in MPa, t-t_1 is the elapsed time after the arrival of the shock wave in micro second, θ is the time constant (when pressure is equal to P_{max}/e) in micro second, R is the standoff distance in m, W is the mass of the spherical TNT explosive in kg.

2.2 Cavitation

Cavitation is defined as a phenomenon that occurs in water led by the reflection of a shock wave at the surface (Wood 1998). Two types of cavitation can occur during an underwater explosion event (UNDEX). The local cavitation occurs at the fluid-structure interface and the bulk cavitation occurs near the free surface and can cover a relatively large area (Ucar 2006).

In general, a fluid cannot withstand tensile stresses when it exceeds significantly and it is likely to undergo large volume expansion when the absolute pressure is close to or less than zero. This phenomenon could be modeled through a cavitation pressure limit for the acoustic medium. When the fluid absolute pressure (sum of the dynamic and initial static pressures) reduces to this limit, the fluid undergoes free volume expansion, without a further drop in the pressure. The constitutive behavior for an acoustic medium capable of undergoing cavitation can be stated as

$$p = \max\{p_v, p_c - p_0\} \tag{4}$$

where, p_v is the pseudo-pressure defined as

$$p_v = -K_f \varepsilon_v \tag{5}$$

where, p_c is the fluid cavitation limit, p_0 is the initial acoustic static pressure, ε_v is the compressive volumetric strain; and K_f is the fluid bulk modulus. When cavitation is considered, a total wave formulation is used to model a nonlinear acoustic medium undergoing cavitation. This formulation is nearly analogous to the scattered wave formulation. The product of the bulk modulus and the compressive volumetric strain called pseudo-pressure plays the role of the material state variable instead of the acoustic dynamic pressure which is readily available from this pseudo-pressure subjected to the cavitation condition. In this study, the cavitation limit parameter is set to zero.

3. Dam body material nonlinearity and contraction joints

Concrete damage plasticity is used to model the dam body material nonlinearity behavior. In this model, damage variables d_t (tension) and d_c (compression) defined independently for assessment of concrete damage and the stiffness degradation are formulated using the damage mechanics approach in continuum domain so that, the main two failure mechanisms are tensile cracking and compressive crushing of the concrete material (Jankowiak and Lodygowski 2005).

The contraction joints are modeled using the small-sliding contact feature. In the small-sliding contact theory, the contacting surfaces can undergo only relatively small sliding relative to each other, but arbitrary rotation of the bodies is permitted. We are able to assign master and slave roles for each two contact surfaces (Labibzadeh and Khajehdezfuly 2011).

4. Boundary and initial conditions

4.1 Dam-reservoir interface and reservoir-reservoir bed interface

The interactions between the structure and foundation surrounding the reservoir and fluid meshes are defined using a surface-based tie constraint; therefore, the interface of the dam and reservoir and also the reservoir and reservoir's bed are constrained so that the normal velocities of the interface nodes are the same in the two-adjacent media.

4.2 Free surface of reservoir

Effects of surface waves are neglected and the boundary condition at the free surface is assigned so that $p=0$, in which p is the pressure.

4.3 Non-reflecting boundary

Created waves cross the boundary and do not return back to the medium. The boundary traction for the transient radiation boundary condition, which is located at the truncated far end of the reservoir, is applied by specifying the corresponding impedance (EmamZadeh 2008)

$$T(x) = -(\frac{1}{c_1}\dot{p} + \frac{1}{a_1}p) \tag{6}$$

$$\frac{1}{c_1} = \left[\frac{f}{\sqrt{\rho_f K_f}}\right] \tag{7}$$

$$\frac{1}{a_1} = f\left[\frac{\beta}{\rho_f} + \frac{\gamma}{2\rho_f\sqrt{\rho_f K_f}}\right] \tag{8}$$

where, ρ_f is the density of the fluid, γ is the volumetric drag (force per unit volume per velocity), K_f is the bulk modulus of the fluid, f is a geometric factor related to the metric factors of the curvilinear coordinate system used on the boundary; and β is a spreading loss term.

4.4 Fluid-structure interaction

Interaction between the reservoir and the structure is defined using a surface-based tie constraint. The transient expressions for the coupled acoustic-structural problem are given as

$$\left(M_f^{PQ} + M_{fr}^{PQ}\right)\ddot{p}^Q + \left(C_f^{PQ} + C_{fr}^{PQ}\right)\dot{p}^Q + \left(K_f^{PQ} + K_{fr}^{PQ} + K_{fi}^{PQ}\right)p^Q = S_{fs}^{PM}T^M + P_f^P \tag{9}$$

$$I^N + M^{NM}\ddot{u}^M + C_{(m)}^{NM}\dot{u}^M = -\left[S_{fs}^{QN}\right]^T p^Q + P^N \tag{10}$$

$$M_f^{PQ} = \int_{V_f} \frac{1}{K_f} H^P H^Q dV \tag{11}$$

$$M_{fr}^{PQ} = \int_{S_{fr} \cup S_{frs}} \frac{1}{K_1} H^P H^Q dS \tag{12}$$

$$C_f^{PQ} = \int_{V_f} \frac{\gamma}{\rho_f}\frac{1}{K_f} H^P H^Q dV \tag{13}$$

$$C_{fr}^{PQ} = \int_{S_{fr} \cup S_{frs}} \left(\frac{\gamma}{\rho_f}\frac{1}{K_1} + \frac{1}{c_1}\right) H^P H^Q dS + \int_{S_{fi}} \frac{1}{c_1} H^P H^Q dS \tag{14}$$

$$K_f^{PQ} = \int_{V_f} \frac{1}{\rho_f}\frac{\partial H^P}{\partial x}\frac{\partial H^Q}{\partial x} dV \tag{15}$$

$$K_{fr}^{PQ} = \int_{S_{fr} \cup S_{frs}} \frac{\gamma}{\rho_f}\frac{1}{c_1} H^P H^Q dS \tag{16}$$

$$K_{fi}^{PQ} = \int_{S_{fi}} \frac{1}{a_1} H^P H^Q dS \tag{17}$$

$$S_{fs}^{PM} = \int_{S_{fs} \cup S_{frs}} H^P \bar{n}.N^M dS \tag{18}$$

$$P_f^P = \int_{S_{ft}} \frac{1}{a_1} H^P T_0 dS \tag{19}$$

$$M^{MN} = \int_V \rho N^N.N^M dV \tag{20}$$

$$C_{(m)}^{MN} = \int_V \alpha_c \rho \, N^N . N^M dV \tag{21}$$

$$I^N = \int_V \beta^N . \sigma dV \tag{22}$$

$$P^N = \int_{S_t} N^N . t dS \tag{23}$$

where, H and N are the fluid and structure element shape functions, respectively, α_c is the damping ratio; and n^- is the normal vector pointing into the fluid. The fluid-solid surface consists of the union of the directly coupled fluid-solid region, S_{fs}, and, S_{frs}. S_{fi} is the radiating acoustic boundary, S_{frs} is a region coupled via a "reactive" acoustic surface or impedance boundary, S (EmamZadeh 2008).

5. Finite element modeling

In the current study, the Karaj Dam (see Fig. 1), which is a double curvature arch dam, is chosen to study the underwater explosion problem. The dam body and foundation are modeled with 8-node linear elements having 3 degrees of freedom in x, y and z directions. The foundation rock is modeled spherically, with the radius of about 2 times the height of the dam body. The length of the modeled reservoir is about 126 m in the upstream direction (Amirpour 2008) and is meshed with 8-node linear elements having one pressure degree of freedom at each node, simulating the acoustic wave propagation. Figs. 2-4 show the provided finite element models for the considered system.

Fig. 1 Downstream view of the Karaj Dam

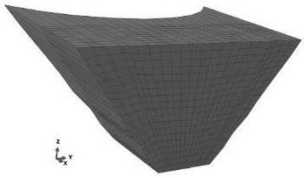

Fig. 2 The finite element mesh of the reservoir

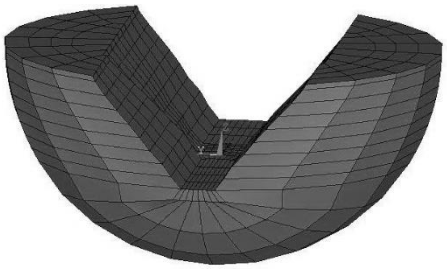

Fig. 3 The finite element mesh of the foundation rock

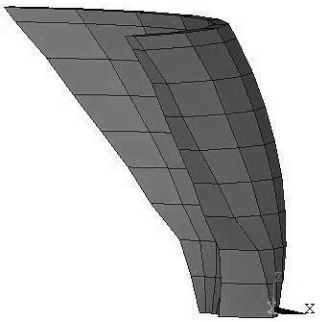

Fig. 4 The finite element mesh of the dam body

The general principle to determine the size of the fluid elements is $L_{max}<C/(n.f_{max})$, where L_{max} is the maximum permitted length of the fluid element, f_{max} is the upper frequency range of the shockwave, C is the acoustic speed within the fluid, and n is the wave number of the shockwave within the element ($n\geq6$) (Jen and Tai 2010).

5.1 Material properties

The modulus of elasticity, Poison's ratio, compressive and static tensile strength for mass concrete are 25 GPa, 0.2, 50 MPa and 3.65 MPa, respectively and its density is taken 2400 kg/m^3. The apparent and dynamic tensile strength assumed for mass concrete are 4.92 MPa and 5.6 MPa, respectively. The assumed foundation rock deformation modulus, its density and Poison's ratio are 16.3 GPa, 3000 kg/m^3 and 0.16, respectively.

5.2 Loading

The applied loads on the provided finite element model are; the self-weight relevant to the dam body, the hydrostatic load in normal water level (160 m from the base of the dam body) and then, the incident waves due to underwater explosion. The incident wave load is applied from the standoff point. It should be noted that only the outer acoustic surfaces should be loaded with the incident wave in total wave formulation, and the incident wave source must be located exterior to the fluid medium (Wood 1998).

6. Numerical results

Four analyses were conducted for considering the effect of underwater explosion on the dam body structural response, which are:

- Linear analysis
- Nonlinear analysis including joints nonlinearity with linear behavior of mass concrete
- Nonlinear analysis including material nonlinearity without considering vertical contraction joints
- Nonlinear analysis including joints and material nonlinearities

The results obtained from various amounts of explosives; 500, 1000,750 and 1500 kg of TNT located at a distance of 200 m from the upstream face of the dam body and for 500 kg TNT at two different distances were studied and compared.

6.1 Analysis 1: Linear analysis

Fig. 6 compares the radial displacement of the dam crest at the crown cantilever (node number 243 as shown in Fig. 5). The maximum crest displacement due to explosion of 500 kg TNT located at a distance of 200 m is less than explosion at a distance of 110 m. As it can be seen, by increasing the distance of explosion source from the dam, the maximum crest displacement is smaller, the behavior which is expected.

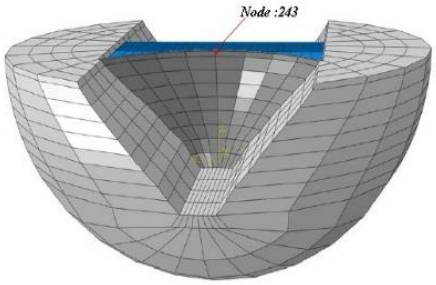

Fig. 5 The location of the node at the crest

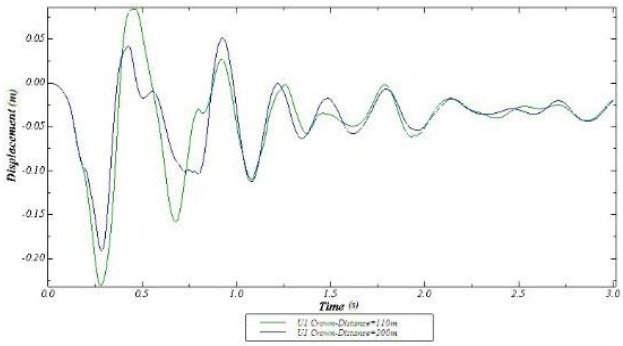

Fig. 6 Radial displacement of the dam crest due to explosion of 500 kg TNT at a distance of 110 m and 200 m

Figs. 7-9 show the crest displacement time histories during the explosion when the explosive weight varies between 500 kg to 1500 kg.

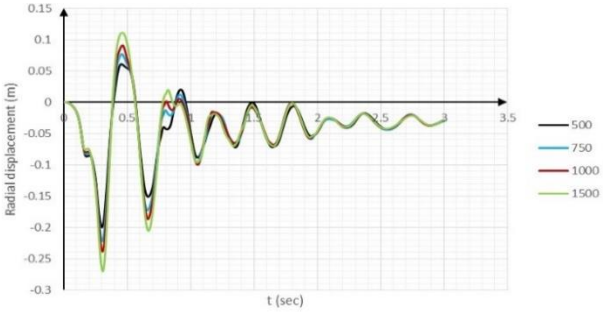

Fig. 7 Radial displacement of the dam crest due to different amount of TNT at a distance of 200 m

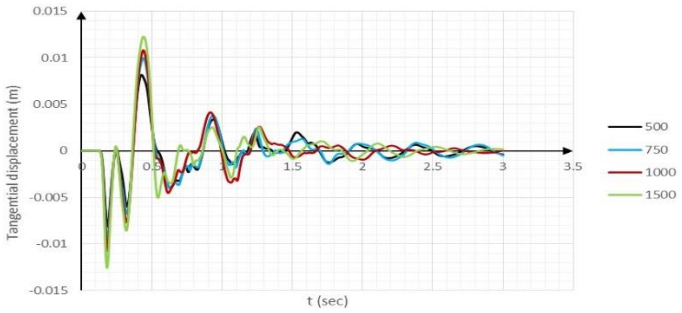

Fig. 8 Tangential displacement of the dam crest due to different amount of TNT at a distance of 200 m

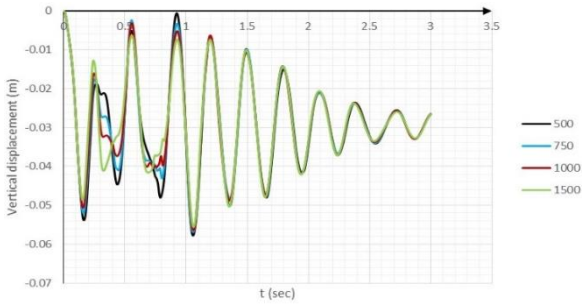

Fig. 9 Vertical displacement of the dam crest due to different amount of TNT at a distance of 200 m

By incremental increase of the weight of explosive, the crown crest displacement will increase. However, there is not a considerable change in the crest movement range resulted from the various weights of explosive in the vertical direction.

Because of concrete elastic behavior, it is expected that the dam crest displacement (tangential and radial displacement) come back to its initial condition (displacement caused by the hydrostatic pressure and the self-weight) after the explosion. This can be seen in the Figs. 7-8. Figs. 10-11 show the contour of the maximum and minimum principal stresses corresponding to the model including 500 kg of TNT located at the distance of 200 m upstream of the dam body. As can be seen, the maximum tensile and compressive stresses within the dam body reach to 10.3 MPa and 18.7 MPa, respectively and therefore, some tensile damages in the dam body are expected. Obviously, the extreme values of the stresses increase with the higher weight of explosive, which have not been shown herein.

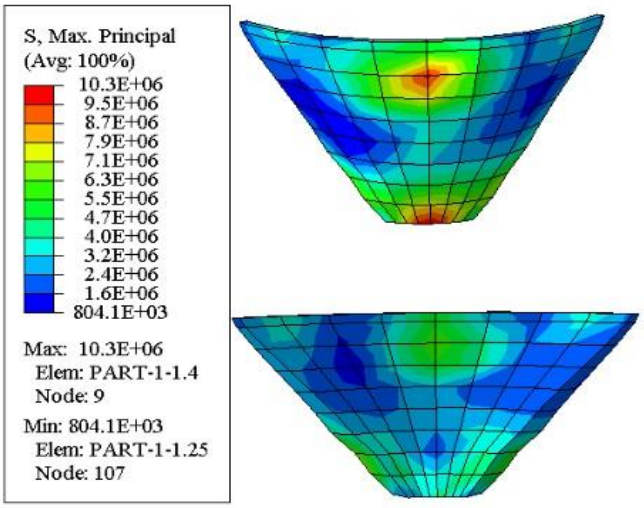

Fig. 10 Maximum principal stress distribution when the maximum crest displacement occurred (500 kg TNT at a distance of 200 m)

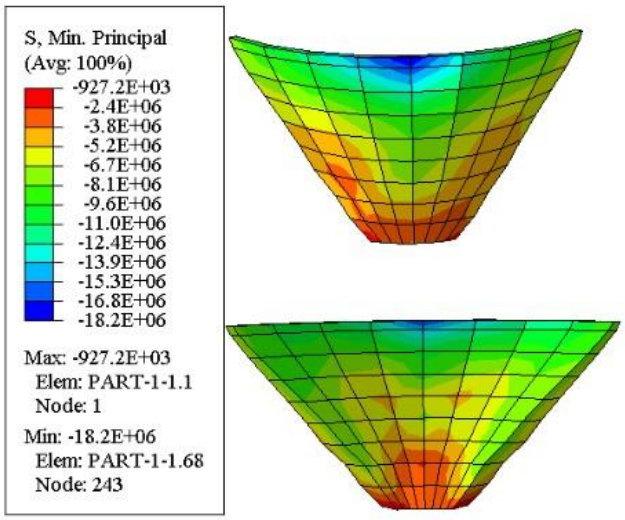

Fig. 11 Minimum principal stress distribution when the maximum crest displacement occurred (500 kg TNT at a distance of 200 m)

6.2 Analysis 2: Joints nonlinearity with linear behavior of mass concrete

In this section, by placing three vertical contraction joints between the blocks of mass concrete embedded in the arch dam body, the analyses are repeated. The behavior of concrete is assumed to be linear. The same as done previously, the explosive weight varies between 500 kg to 1500 kg and the crest displacement histories are shown in Figs. 12-14. Furthermore, the maximum and minimum principal stress distributions are shown in Figs. 15-16 corresponding to the model including 500 kg of TNT located at the distance of 200 m upstream of the dam body.

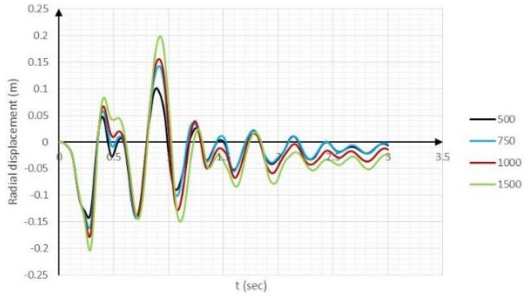

Fig. 12 Radial displacement of the dam crest due to different amount of TNT at a distance of 200 m

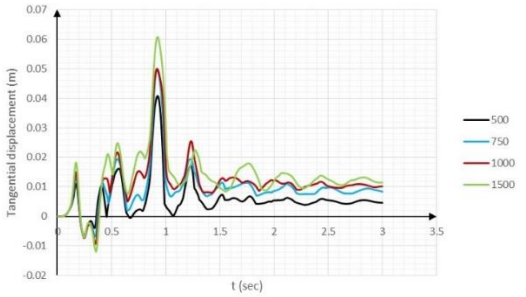

Fig. 13 Tangential displacement of the dam crest due to different amount of TNT at a distance of 200 m

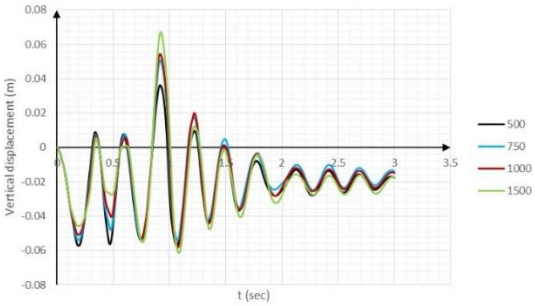

Fig. 14 Vertical displacement of the dam crest due to different amount of TNT at a distance of 200 m

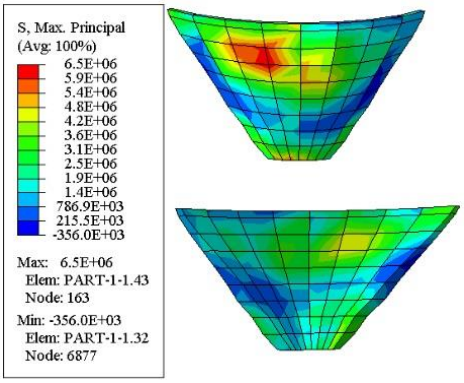

Fig. 15 Maximum principal stress distribution when the maximum crest displacement occurred (500 kg TNT at a distance of 200 m)

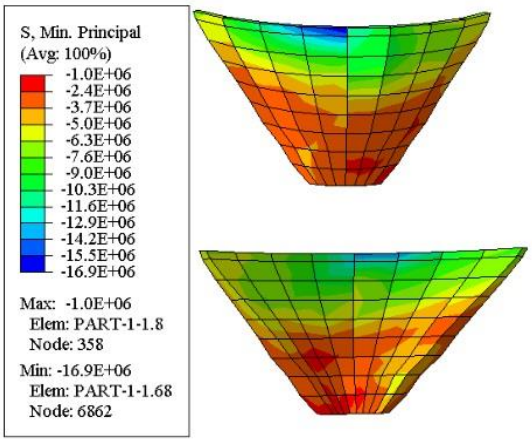

Fig. 16 Minimum principal stress distribution when the maximum crest displacement occurred (500 kg TNT at a distance of 200 m)

Like as seen in linear analysis, by incremental increase of the weight of explosive, the crown crest displacement (radial and tangential displacement) will increase. Furthermore, unlike linear analysis, there is a considerable change in the maximum crest movement range resulted from the various weights of explosive in the vertical direction. Because of joints placement, the dam crest displacement (tangential and radial displacement) does not come back to its initial condition after the explosion and there are some small residual deformations.

Based on Figs. 7-9 and Figs. 12-14, up to 0.5 s of analysis, all components of the crown displacements are the same for the analysis cases with and without joints; however, after 0.5 s, these components of displacements will increase significantly in the model including contraction joints. In fact, after 0.5 s of analysis, the joints are opened and thereupon, the results of two analyses are different.

Furthermore, by joints placement, there is more sensitivity due to an explosive weight change but its change rate for vertical displacement is lower in comparison with the radial and tangential displacements.

Comparing with the linear analysis, the maximum principal stresses will reduce but the minimum principle stresses will not change significantly. It can be concluded that the contraction joints will be separated under tensile stresses while as a result there will be more displacements and less tensile stresses. It can be concluded that the contraction joints will reduce stresses but make the structures more flexible. Furthermore, maximum of tensile stresses are at the middle of the dam body during the linear analysis; however, in the case with the contraction joints, these maximum stresses will shift toward abutments. It must be mentioned that the values of tensile stresses are changed near the contraction joints and by more distances from the contraction joints, these differences will be less.

6.3 Analysis 3: Material nonlinearity without vertical contraction joints

In this section, the concrete damage Plasticity model is used and the damage variables are computed but there is no joint in the dam body. Figs. 17-19 show the crest displacement time histories during the explosion.

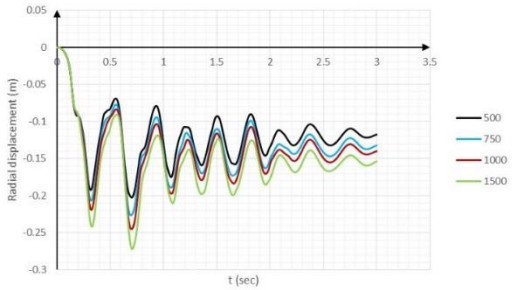

Fig. 17 Radial displacement of the dam crest due to different amount of TNT at a distance of 200 m

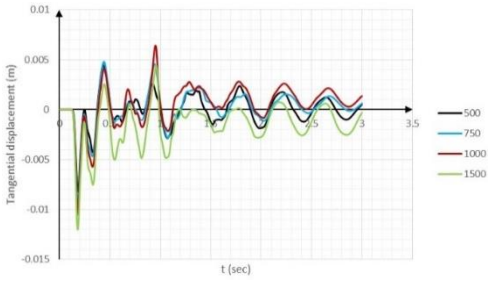

Fig. 18 Tangential displacement of the dam crest due to different amount of TNT at a distance of 200 m

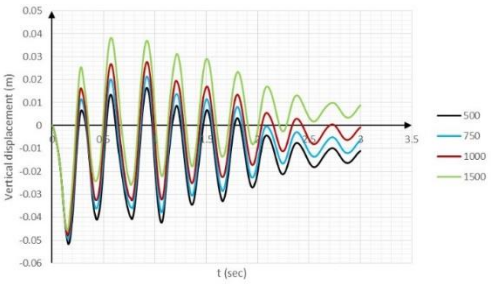

Fig. 19 Vertical displacement of the dam crest due to different amount of TNT at a distance of 200 m

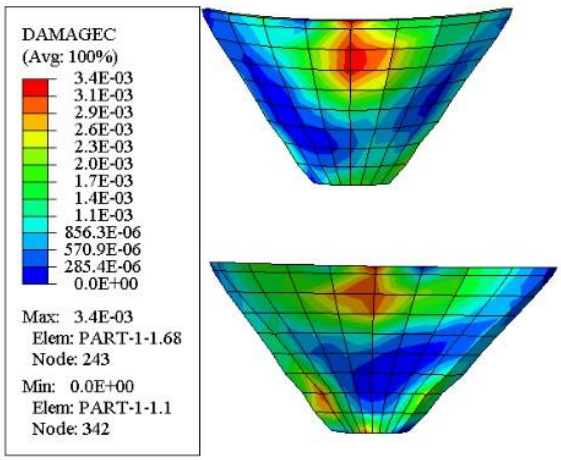

Fig. 20 dc distribution when the maximum crest displacement occurred (500 kg TNT at a distance of 200 m)

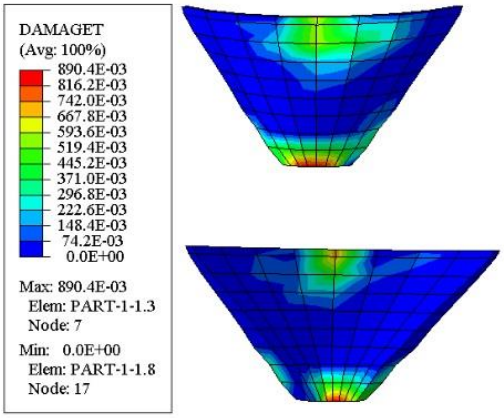

Fig. 21 dt distribution when the maximum crest displacement occurred (500 kg TNT at a distance of 200 m)

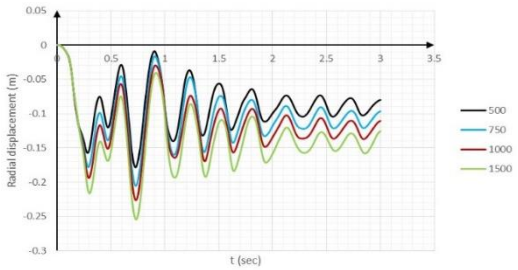

Fig. 22 Radial displacement of the dam crest due to different amount of TNT at a distance of 200 m

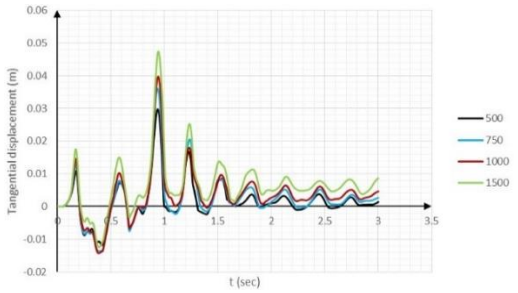

Fig. 23 Tangential displacement of the dam crest due to different amount of TNT at a distance of 200 m

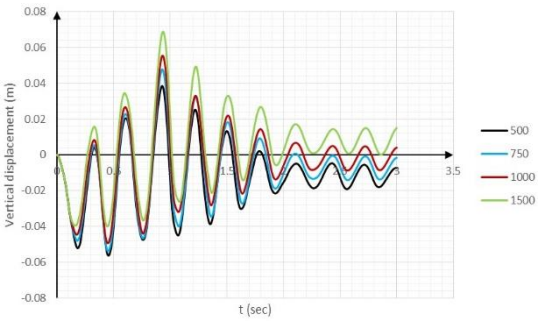

Fig. 24 Vertical displacement of the dam crest due to different amount of TNT at a distance of 200 m

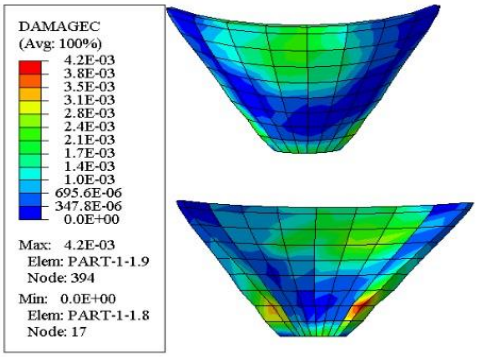

Fig. 25 dc distribution when the maximum crest displacement occurred (500kg TNT at a distance of 200 m)

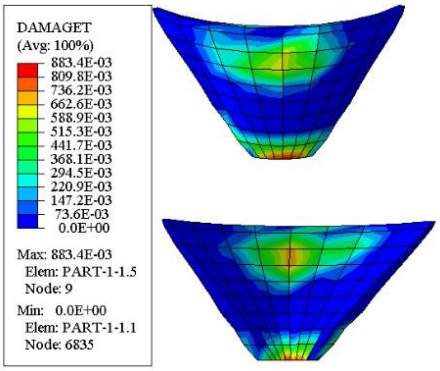

Fig. 26 dt distribution when the maximum crest displacement occurred (500 kg TNT at a distance of 200 m)

As shown in Figs. 17-19 and Figs. 7-9, the crown displacements are more sensitive to the amount of TNT in the conducted nonlinear analysis. Furthermore, up to the time of 0.25 s (approximately), there is not any difference between the two categories of the crown displacement (linear and nonlinear analysis). It can be concluded that before 0.25 s, there is not any nonlinear behavior in the dam body. But after 0.25 s of analysis, the radial and vertical displacements will increase substantially and tangential displacement will reduce.

As shown in Fig. 20, d_c, as the damage variable in compression (varying from 0 to 1) is approximately zero but there are substantial damages under the tensile stresses (Fig. 21). It can be concluded that the assumption of linear analysis under compressive conditions will not change our results but the nonlinear behavior due to the tensile stresses is essential. It is worth mentioning that maximum of d_c will happen at the place of minimum compressive stresses for linear analysis and maximum of d_t (as the damage variable in tension) will happen at the place of maximum tensile stresses of linear analysis.

6.4 Analysis 4: Nonlinear analysis including joints and material nonlinearities

In these series of conducted analyses, the dam body includes the contraction joints and material nonlinearity is assumed for mass concrete and different amount of TNT are considered at a distance of 200 m from the dam body and results are studied (see Figs. 22-26).

Comparing the results shown in Figs. 22-24 with those shown in Figs. 12-14 corresponding with the cases including just joint nonlinearity, up to 0.25 s (approximately) there is not any difference between the results, so the same as the last analyses before 0.25 s, there is not any nonlinear behavior in the dam body. Therefore, by joints placement, the onset of nonlinear behavior moment will not change significantly. As it was mentioned, linear dam body will come back to its initial value and it will oscillate between these initial values. But by assignment of nonlinear behavior, there are some residual radial displacements in the dam body and the structure will oscillate between these final values. Furthermore, by assignment of nonlinear behavior, the dam responses are more sensitive to the explosive weight.

6.5 Hydrodynamic pressure

The following figure depicts the contours of PABS (the absolute pressure, equal to the sum of the total dynamic acoustic pressure and the hydrostatic pressure) at several time instants. The hydrostatic pressure at the first time and the propagation of the shockwave in the fluid due to 1500 kg TNT at a distance of 200 m from the dam are shown in Figs. 27-33 along the reference plane of the dam body geometry.

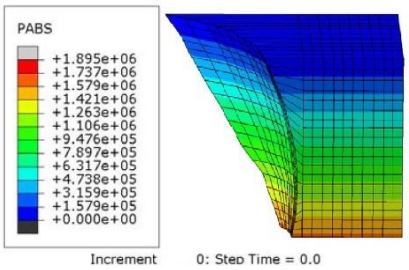

Fig. 27 Hydrodynamic pressure at time=0.0

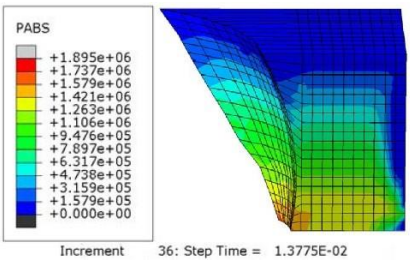

Fig. 28 Hydrodynamic pressure at time=1.3775E-02

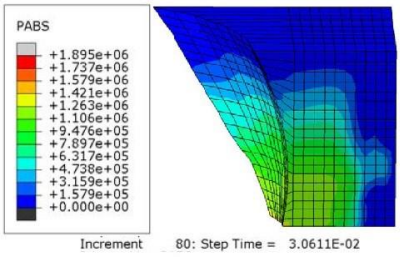

Fig. 29 Hydrodynamic pressure at time=3.0611E-02

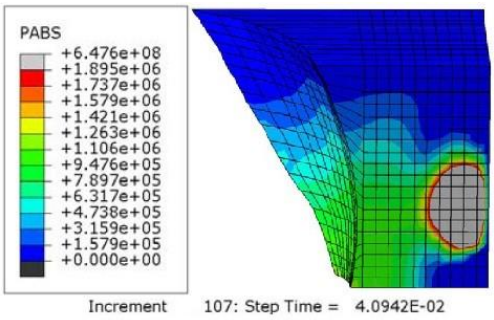

Fig. 30 Hydrodynamic pressure at time=4.0942E-02

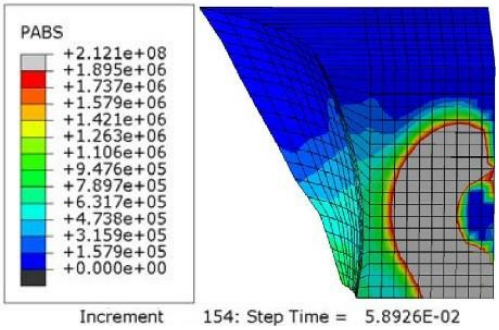

Fig. 32 Hydrodynamic pressure at time=5.88926E-02

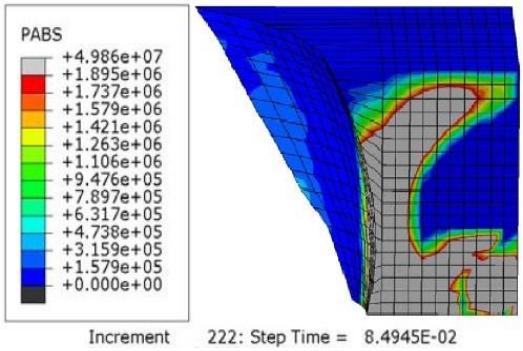

Fig. 33 Hydrodynamic pressure at time=8.4945E-02

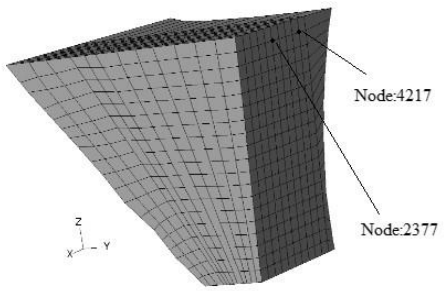

Fig. 34 The location of the nodes to represent the hydrodynamic pressure

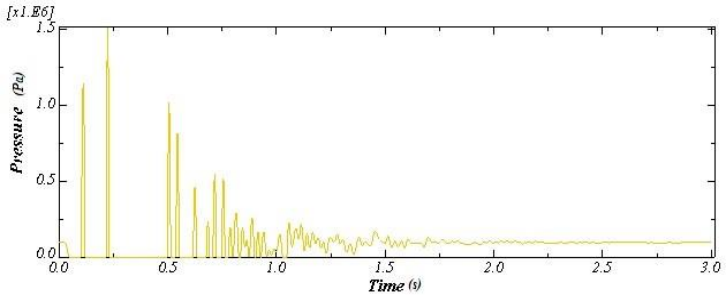

Fig. 35 Hydrodynamic pressure changes at nodes 2377

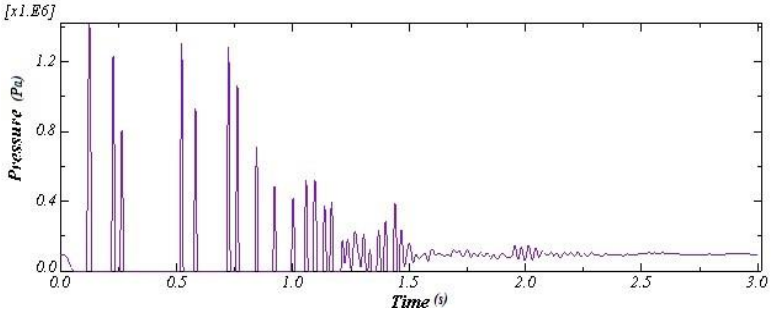

Fig. 36 Hydrodynamic pressure changes at nodes 4217

Hydrodynamic pressure changes at nodes 2377 and 4217 (see Fig. 34) are shown in Figs. 34 and 36. As can be seen in these figures, the pressure at the beginning of the analysis is equal to the hydrostatic pressure and after fluctuation come back to it again.

7. Conclusions

In the current study, Karaj double curvature arch dam is loaded having underwater explosion. The dam body is assumed with and without contraction joints and linear and nonlinear material behavior are assumed and four types of analyses are conducted. The dam body material nonlinearity is simulated using damage plasticity model.

• As expected, the maximum crest displacement will decrease by increasing the distance of explosion source. In the linear analysis, there isn't any residual displacement after explosion because of concrete elastic behavior.

• Comparing nonlinear analyses with and without joints, it can be concluded that joints are opened at 0.2 s; Up to 0.2 s, the crown displacement components are the same. But subsequently, by joints placement, the amplitude of the crown displacements will increase. The tangential displacements are more affected in comparison with the other two displacement components.

• Comparing d_c and d_t (Figs. 25-26), the same as nonlinear analysis without joints, the dam body is damaged substantially under the tensile stresses; but under the compressive stresses there is not any substantial damage to the dam body.

• Comparing d_t resulted from the nonlinear analyses with and without joints, it seems that joints placement (Fig. 26) will not change d_t value at the bottom of the dam body on the upstream and

downstream faces and on the upstream face of the dam crown. However, at the crown of the dam body on the downstream face, d_t will have larger values at mid parts of the dam body.

• The dam body is safe under the loads considered in the current study and there is not any significant or notable structural damage after explosions considered in this study.

References

Amirpour, A. (2008), "Performance seismic evaluation of arch dams including foundation dam reservoir with endurance time method", M.Sc. Dissertation, K.N.Toosi University OF Technology, Tehran, Iran.

Cole, R.H. (1948), *Underwater Explosions*, Princeton University Press, Princeton, New Jersey, U.S.A.

EmamZadeh, S. (2008), "An adaptive finite element analysis of acoustic waves propagation due to underwater explosion for fluid-structure interaction problems", Ph.D. Dissertation, Tarbiat Modarres University, Tehran, Iran.

Ghanaat, Y., Hall, R.L. and Redpath, B.B. (2000), "Measurement and computation of dynamic response of arch dams including interaction effects", *J. Seismol. Earthq. Eng.*, **2**(3), 41-54.

Hakan Ucar, H. (2006) "Dynamic response of a catamaran-hull ship subjected to underwater explosions", M.Sc. Dissertation, Naval Postgraduate School, Monterey, California, U.S.A.

Jankowiak, T. and Lodygowski, T. (2005), "Identification of parameters of concrete damage plasticity constitutive model", *Foundat. Civil Environ. Eng.*, **6**(1), 53-69.

Jen, C.Y. and Tai, Y.S. (2010), "Deformation behavior of a stiffened panel subjected to underwater shock loading using the non-linear finite element method", *Mater. Des.*, **3**(1), 325-335.

Junxiang, X. and Xila, L. (2008), "Full coupled simulation of concrete dams subjected to underwater Explosion", *J. Shanghai Jiaotong Univ.*, **42**(6), 1001-1004.

Kwon, Y.W. and Fox, P.K. (1993), "Underwater shock response of a cylinder subjected to a side-on explosion", *Comput. Struct.*, **48**(4), 637-646.

Labibzadeh, M. and Khajehdezfuly, A. (2011), "Effect of vertical contraction joints on thermo-static stability of karun-1 arch dam", *Trend. Appl. Sci. Res.*, **6**(1), 34-46.

McCoy, R.W. and Sun, C.T. (1997), "Fluid-structure interaction analysis of a thick section composite cylinder subjected to underwater blast loading", *Compos. Struct.*, **37**(1), 45-55.

Qiankun, J. and Gangyi, D. (2011), "A finite element analysis of ship sections subjected to underwater explosion", *Int. J. Imp. Eng.*, **38**(7), 558-566.

Rajendran, R. and Narasimhan, K. (2006), "Deformation and fracture behaviour of plate specimens subjected to underwater explosion-a review", *Int. J. Imp. Eng.*, **32**(12), 1945-1963.

Salajegheh, E., Salajegheh, J. and Biglarkhani, M. (2008), "Dynamic response of spar platform subjected to far-field underwater shock", *Proceedings of the 4th National Conference on Civil Engineering*, University of Tehran, Iran.

Shah Mohammadi, H. and Mohammadi, S. (2010), "Analysis of blast shock waves on immersed pipes", *Civil Eng. Infrastruct. J.*, **44**(1), 61-72.

Wood, S.L. (1998), "Cavitation effects on a ship-like box structure subjected to an underwater explosion", M.Sc. Dissertation, Naval Postgraduate School, Monterey, California, U.S.A.

Yu, T. (2009), "Dynamical response simulation of concrete dam subjected to underwater contact explosion load", *Proceedings of the WRI World Congress on Computer Science and Information Engineering*.

Zhu, F., Zhu, W.H., Zhu, X., Sun, J.B. and Hua, X. (2012), "Numerical simulation of arch dam withstand underwater explosion", *Proceedings of the International Conference on IEEE in Modelling, Identification & Control (ICMIC).*